Mass-manufacturable scintillation-based optical fiber dosimeters for brachytherapy

Gierej, A., Baghdasaryan, T., Martyn, M., Woulfe, P., Mc Laughlin, O., Prise, K., Workman, G., O'Keeffe, S., Rochlitz, K., Verlinski, S., Giaz, A., Santoro, R., Caccia, M., Berghmans, F., & Van Erps, J. (2024). Mass-manufacturable scintillation-based optical fiber dosimeters for brachytherapy. *Biosensors and Bioelectronics*, *255*, Article 116237. https://doi.org/10.1016/j.bios.2024.116237

Document Version:
Peer reviewed version

Queen's University Belfast - Research Portal:
Link to publication record in Queen's University Belfast Research Portal

Journal Pre-proof

Mass-manufacturable scintillation-based optical fiber dosimeters for brachytherapy

Agnieszka Gierej, Tigran Baghdasaryan, Michael Martyn, Peter Woulfe, Owen Mc Laughlin, Kevin Prise, Geraldine Workman, Sinead O'Keeffe, Kurt Rochlitz, Sergey Verlinski, Agnese Giaz, Romualdo Santoro, Massimo Caccia, Francis Berghmans, Jürgen Van Erps

Please cite this article as: Gierej, A., Baghdasaryan, T., Martyn, M., Woulfe, P., Mc Laughlin, O., Prise, K., Workman, G., O'Keeffe, S., Rochlitz, K., Verlinski, S., Giaz, A., Santoro, R., Caccia, M., Berghmans, F., Van Erps, Jü., Mass-manufacturable scintillation-based optical fiber dosimeters for brachytherapy, *Biosensors and Bioelectronics* (2024), doi: https://doi.org/10.1016/j.bios.2024.116237.

This is a PDF file of an article that has undergone enhancements after acceptance, such as the addition of a cover page and metadata, and formatting for readability, but it is not yet the definitive version of record. This version will undergo additional copyediting, typesetting and review before it is published in its final form, but we are providing this version to give early visibility of the article. Please note that, during the production process, errors may be discovered which could affect the content, and all legal disclaimers that apply to the journal pertain.

Mass-Manufacturable Scintillation-Based Optical Fiber Dosimeters for Brachytherapy

Agnieszka Gierej[1], Tigran Baghdasaryan[1], Michael Martyn[2,6], Peter Woulfe[2], Owen Mc Laughlin[3], Kevin Prise[3], Geraldine Workman[3], Sinead O'Keeffe[4], Kurt Rochlitz[1], Sergey Verlinski[1], Agnese Giaz[5], Romualdo Santoro[5], Massimo Caccia[5], Francis Berghmans[1], and Jürgen Van Erps[1]

[1] Brussels Photonics (B-PHOT), Vrije Universiteit Brussel and Flanders Make, Dept. of Applied Physics and Photonics, Brussels, Belgium.
[2] Department of Medical Physics, Blackrock Health – Galway Clinic, Doughiska, Co. Galway, Ireland.
[3] The Centre for Cancer Research & Cell Biology (CCRCB) at Queen's University Belfast, UK.
[4] Optical Fibre Sensors Research Centre, University of Limerick, Ireland.
[5] Università degli Studi dell'Insubria, Dipartimento di Scienza e Alta Tecnologia, via Valleggio 11, Como, Italy
[6] Physics Unit, School of Natural Sciences, University of Galway, Galway, Ireland

E-mail: jurgen.van.erps@vub.be

Abstract

Scintillation-based fiber dosimeters are a powerful tool for minimally invasive localized real-time monitoring of the dose rate during Low Dose Rate (LDR) and High Dose Rate (HDR) brachytherapy (BT). This paper presents the design, fabrication, and characterization of such dosimeters, consisting of scintillating sensor tips attached to polymer optical fiber (POF). The sensor tips consist of inorganic scintillators, i.e. $Gd_2O_2S:Tb$ for LDR-BT, and $Y_2O_3:Eu+4YVO_4:Eu$ for HDR-BT, dispersed in a polymer host. The shape and size of the tips are optimized using non-sequential ray tracing simulations towards maximizing the collection and coupling of the scintillation signal into the POF. They are then manufactured by means of a custom moulding process implemented on a commercial hot embossing machine, paving the way towards series production. Dosimetry experiments in water phantoms show that both the HDR-BT and LDR-BT sensors feature good consistency in the magnitude of the average photon count rate and that the photon count rate signal is not significantly affected by variations in sensor tip composition and geometry. Whilst individual calibration remains necessary, the proposed dosimeters show great potential for in-vivo dosimetry for brachytherapy.

Keywords: inorganic scintillators, radiation sensor, brachytherapy, optical fiber, compression moulding

1. Introduction

Within the dynamic landscape of medical instrumentation, optical sensors have become instrumental in providing real-time monitoring solutions for medical applications. This paper delves into the intricacies of designing, fabricating, and evaluating scintillation-based optical fiber dosimeters crafted to meet the specific requirements of brachytherapy (BT). BT is a form of radiotherapy which is commonly employed for the treatment of cancer [1], referring to the use of radioactive sources that are implanted within, or in close proximity to the critical target organ. We focus here on BT for prostate or cervical cancer. BT can be divided into two categories, based on the dose rate of the employed radioactive source, with low-dose-rate (LDR) and high-dose-rate (HDR) BT employing sources with dose rates of < 2 and > 12 Gy/h, respectively [2].

The distinct advantage of optical sensors lies in their minimally intrusive nature, allowing for localized monitoring of the dose rate at specific locations in the vicinity of the tumerous tissue. In the context of BT, where precision in dose delivery is paramount in view of accurately determining the radiation dose delivered to critical organs near the treatment zone, such as the bladder, the urethra and the rectal wall during radiation treatment [3], optical fiber dosimeters offer a solution aligning with the principles of precision, miniaturization, and real-time feedback. A substantial amount of research has been conducted to develop such fiber-optic dosimeters [4-11]. Fiber-optic scintillation-based dosimeters are compact and radiation-resistant devices that are used for real-time monitoring of the dose rate at specific locations in the vicinity of tumorous tissue during BT radiation treatment of prostate or cervical cancer. These dosimeters are based on scintillators, which are materials that emit light when exposed to ionizing radiation. The scintillation light is collected by an optical fiber, which transmits the optical signal to a photodetector and dedicated electronic circuitry for further signal processing. Fiber-optic scintillation-based dosimeters have several advantages over other types of dosimeters,

including their compact size, real-time response proportional to the absorbed dose-rate in their sensitive volume, water equivalence, and insensitivity to magnetic fields [6].

Our study concentrates on the development of dosimeters incorporating scintillating sensor tips integrated with polymer optical fiber (POF). Inorganic scintillators are preferred over organic scintillators owing to their larger X-ray absorption and higher light output [6]. The selection of inorganic scintillators—Gd_2O_2S:Tb for LDR-BT and Y_2O_3:Eu+4YVO_4:Eu for HDR-BT—embedded in a suitable polymer host to form the sensor tips requires adequately combining material science, fabrication technologies, optics and medical instrumentation requirements. In our case, the sensor tip design is meticulously optimized through non-sequential ray tracing simulations, focusing on maximizing the collection and coupling of scintillation signals into the POF.

Crucially, this paper discusses a custom moulding process executed on a commercial hot embossing machine, showcasing the pathway to series production. This scalability aligns with the community's interests, reflecting the potential for widespread implementation of these dosimeters in clinical settings. Finally, fiber-optic dosimetry experiments conducted in water phantoms yield valuable insights into the dosimeters' performance. Notably, the dosimeters exhibit consistent average photon count rates for both HDR-BT and LDR-BT scenarios, with minimal impact from variations in sensor tip composition and geometry. While individual calibration remains a requisite step, our dosimeters present significant promise for in-vivo dosimetry in brachytherapy, highlighting the transformative role that these optical sensors play in advancing medical applications.

2. Materials and Methods

The tips are fabricated by means of a custom-developed two-step process using a Jenoptik HEX04 hot embossing and compression moulding machine. In the first step, we manufacture substrates consisting of 60% scintillating powder dispersed in 40% PMMA. In the second step, this substrate is used for the manufacturing of multiple scintillating tips per cycle using a custom transfer moulding tool.

2.1. Specification inorganic scintillator, polymer host and polymer optical fiber

The fiber optic BT dosimeters utilize a scintillating sensor tip attached to the end of a polymer optical fiber (POF). These scintillating tips consist of a scintillating inorganic material that initially comes in a powder form that is incorporated within a thermoplastic polymer host, in our case polymethyl methacrylate (PMMA). The choice of scintillators for LDR- and HDR-BT is primarily based on the specific characteristics and requirements of each technique in view of ensuring

accurate and precise dose delivery to the tumor during BT procedures. LDR-BT involves the use of low-activity radioactive sources that emit radiation over an extended period (i.e. hours to days), whilst HDR-BT uses high-activity radioactive sources that emit a very high dose of radiation over a short period (i.e. fractions of seconds to minutes). LDR scintillators are optimized for detecting low-energy gamma radiation (around 25 keV to 35 keV) emitted by sources with longer half-lives, such as Iodine-125 (^{125}I), whereas HDR scintillators are designed to detect high-energy gamma radiation (around 300 keV to 600 keV) from sources with shorter half-lives, such as Iridium-192 (^{192}Ir).

The scintillating materials employed in this study are Gd2O2S:Tb and Y2O3:Eu+4YVO4:Eu for LDR- and HDR-BT, respectively. They are sourced from Phosphor Technology Ltd., U.K. [12]. These materials were chosen for two main reasons, i.e. the spectral content of the scintillation signal and their availability in fine-grained powder. For LDR, the scintillation features three emission peaks with the main peak at 544 nm and two others at 490 nm and 590 nm. For HDR, YVO4:Eu emits at 619 nm, whilst Y2O3:Eu emits at 611 nm. All these emission wavelengths are well separated from the wavelength of Cherenkov radiation [13] and hence allow filtering out the stem-effect [14]. Since neither the scintillation yield nor the decay time of the scintillation is provided by the powder producer and, given that the data reported in literature is inconsistent and exhibits a significant dependence on the stoichiometry of the product, we first conducted an in-depth characterization of the scintillators, of which the results have been documented in [15].

Additionally, these scintillating materials come in grain sizes with an average ~4 μm diameter for LDR, and an average ~7 μm diameter for the HDR. This enables dispersing the powders in a thermoplastic host and consequently the integration in a polymer sensor tip that can be obtained through a thermoforming process. Our sensor tips consist of 60% scintillating powder dispersed in 40% PMMA, as stated above. We manually mixed scintillating powders, i.e. 3 g of Gd2O2S:Tb for LDR, or 3 g of Y2O3:Eu+4YVO4:Eu for HDR with 2 g of PMMA powder sourced from Merck Sigma-Aldrich®. This PMMA has an average molar mass Mw ~15,000 g/mol, and particle sizes ranging from 0.149 mm to 2.0 mm. We call these mixtures respectively LDR-PMMA and HDR-PMMA.

To collect the scintillation signal, we use a POF. Given the need to integrate the probe in a BT catheter system, the POF should have a maximum core diameter of 0.5 mm. To maximize the scintillation signal collection efficiency, the numerical aperture (NA) of the POF should be as high as possible. From a selection of commercially available POFs, we have chosen one with an NA of 0.5 and an uncoated core diameter of 0.5 mm from Jiangsu TX Plastic Optical Fibers Co., Ltd. These step-index POFs were sourced with one fiber

end cut and polished and the second fiber end terminated with an SMA 905 connector. The length of the optical fiber is 5 meters. The POF specifications and dimensions are summarized in Table 1.

Table 1. POF specifications.

Core material	PMMA
Jacket material	PE
Core refractive index	1.492
Numerical aperture	0.5 ± 0.15
Min. bend radius	25 mm
Core diameter	$480 \pm 30 \, \mu m$
Cladding diameter	$500 \pm 30 \, \mu m$
Jacket diameter	$1000 \pm 70 \, \mu m$
Optical loss at 650 nm	<210 dB/km

2.2. Optical modeling of the sensor tip

The performance of radiation dose measurements relying on scintillation-based dosimetry, with scintillation signal collected by means of an optical fiber, obviously depends on how efficiently said signal is captured by and guided within the optical fiber to the photodetector. Therefore, the objective of the optical modeling is to design the scintillating tip such that it complies with the geometrical constraints imposed by the allowed probe dimension whilst providing for a maximized collection of generated scintillation signal and coupling of that signal into the POF with a 0.5 mm-diameter core. Additionally, the scintillating tip should not exceed 3 mm in length to allow for a sufficiently high spatial resolution of the dose measurement. Finally, to ensure compatibility with the envisioned fabrication process, a demoulding angle ($\geq 1°$) should be considered in the design of the sensor tip as well in view of facilitating the extraction of the tip from the fabrication mould.

Given those specifications, we started with designing the shape of the scintillating tip with the aim of collecting the largest amount of scintillating signal as possible by the POF. For this purpose, we built a non-sequential ray tracing model using Zemax® OpticStudio®. Dedicated models were created for the HDR-PMMA and LDR-PMMA mixtures, based on their refractive index and their attenuation. To estimate the refractive indices of these materials, we started from the refractive index of PMMA, i.e. n=1.49 as specified by [16]. The HDR scintillator consists of 4 portions of YVO_4:Eu and 1 portion of Y_2O_3:Eu, with refractive indices of n=2.05 and n=1.9, respectively. This leads to a weighted average refractive index of n=1.81 for the HDR-PMMA compound, given the concentrations of the different constituents. For the LDR-PMMA compound the weighted average refractive index is n=1.98, given that the refractive index of Gd_2O_2S:Tb is n=2.3. An attenuation coefficient of 6.75 dB/mm at 619 nm was implemented in the model for HDR-PMMA, and of 5.08 dB/mm at 544 nm for LDR-PMMA, respectively. These

values were obtained by transmission measurements of the intermediate scintillating substrates using an integrating sphere, taking into account both linearly transmitted and diffused light, fully in line with the methodology described in our previous work [15]. For more details, see Section 1 of the Supplementary Information.

The scintillation events in the sensor tip can be modeled in OpticStudio® by way of individual rays. The generated photons travel in random directions and hence we can consider the source as an isotropic light volume emitter and volume scatterer. A volume emitter assumes that the rays are emitted in random directions from anywhere inside the volume, with uniform probability in both position and ray direction, whilst volume scattering implies the existence of scattering particles of a certain size distributed uniformly with a certain density within the volume. We assume that the scintillation events are uniformly distributed within the volume of the sensor and the amount of light emitted by the scintillating tip increases propotionally with the volume of scintillating material. This allows us to compare different scintillating tip designs by calculating a figure of merit, expressed in arbitrary units (a.u.), based on the amount of optical power coupled into the POF core relative to the volume of the scintillating tip. To reflect this in the simulations, we define the optical power yield from a unit volume (1 mm^3) as 100 a.u./mm^3.

Two scintillating tip geometries were considered for the simulations: (1) a hemispherical tip, as a reference design, with diameter of the hemisphere equal to the POF diameter; and (2) a cylindrical tip, of which the cylinder length can be chosen in view of maximizing the scintillation signal.

If one requires the sensor size to remain within the volume defined by the POF outer diameter, a cylindrical shape is the most straightforward choice, as it optimally fills the volume allocated for the sensor on the fiber tip and maximizes the amount of generated scintillating light. Therefore, we first fixed the diameter of the cylindrically shaped sensor tip to 0.5 mm (corresponding to the POF diameter) and then we optimized the length of the sensor tip. A cylinder with a longer length allows for more scintillation light to be generated. However, because of the optical attenuation in the material, light produced at the edges of the sensor has a lower probability of reaching the POF core. This is shown in Figure 1a, which graphs the optical power coupled into the POF as a function of the length of the cylindrically shaped sensor tip, with the attenuation in the scintillating compounds either being accounted for or neglected. For a lossless scintillating cylindrical tip, the optical power coupled into the POF increases linearly with the length of the. However, when absorption and scattering are accounted for, we observe a saturation in the power coupled into the POF after a certain length. The figure of merit for the cylindrical sensor tip made from HDR-PMMA with a 0.5 mm-diameter (solid blue line) becomes identical to that of the hemispherical tip for a

cylinder length of 0.5 mm, with a coupled power equal to 0.2 a.u.. If we increase the length of the sensor to 1 mm, the coupled power increases to 0.274 a.u. for HDR-PMMA, and 0.271 a.u. for LDR-PMMA (see Fig. 5 in the Supplementary Material), representing a 35% increase in fiber-coupled power as compared to the reference hemispherical shape. Given the saturation of the optical power coupled into the POF, there is no significant increase of coupled power if the length of the scintillating tip is increased beyond 1 mm. This size also complies with the required spatial resolution of the local dose measurement, which should be below 3 mm.
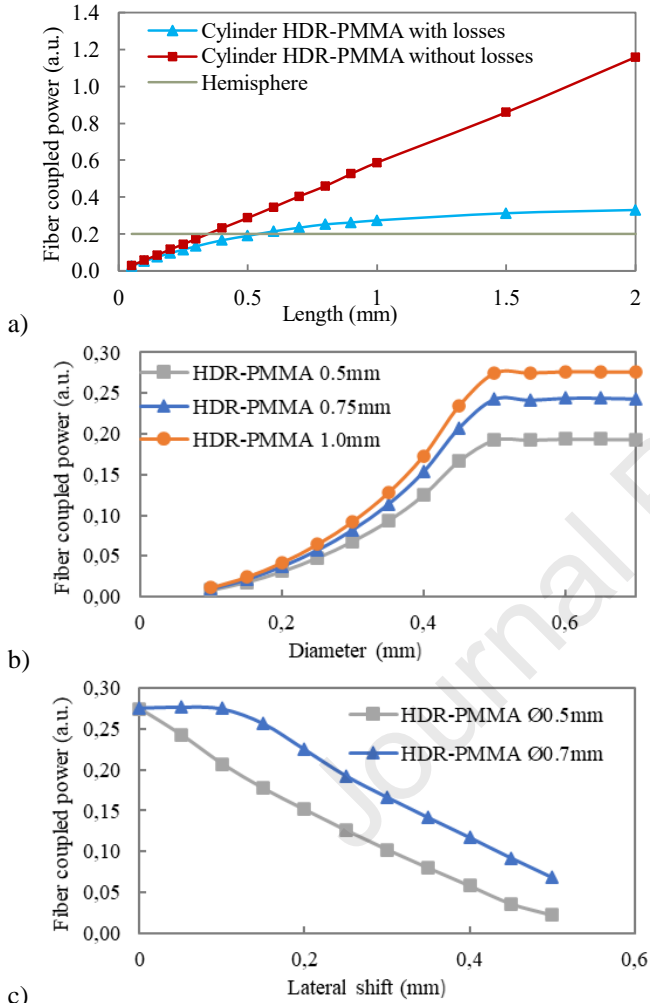

a)

b)

c)

Figure 1. Simulation results for HDR-PMMA: a) Optical power coupled to the 0.5 mm POF for a cylindrically shaped scintillating tip with a 0.5 mm-diameter as a function of the tip length; b) Influence of the diameter of a cylindrically shaped scintillating tip of varying length on the optical power coupled to a 0.5 mm-diameter POF; c) Effect of lateral eccentric misalignment with respect to the center of the POF for a scintillating tip with a length of 1.0 mm (and diameter of 0.5 mm and 0.7 mm) on the optical power coupled to the POF. The results for LDR-PMMA are very similar and are shown in Fig. 5 of the Supplementary Material.

Furthermore, we studied the influence of the cylindrical scintillating tip diameter on the power coupled into the POF. The maximum diameter of the sensor tip was set to 0.7 mm to

ensure that three sensor fibers could be accommodated within the constraints of the smallest available model of Foley catheter, a medical device used for various urology procedures, including drainage and monitoring, without compromising its functionality or safety. Figure 1b shows the simulation results for three different tip lengths (L=0.5 mm, L=0.75 mm and L=1.0 mm) as a function of the sensor tip diameter D. Starting from a diameter D=0.1 mm, the optical power coupled into the 0.5 mm POF increases with D up to D=0.5 mm, beyond which the coupled power remains constant. A sensor tip with a larger diameter therefore does not result in a more efficient sensor in terms of optical power being coupled to the POF core.

However, a scintillating tip with a larger diameter allows for some more relaxed positioning tolerance when attaching the tip to the end facet of the POF, which in turn eases the assembly and likely results in improved repeatability. To quantify the influence of a lateral misalignment of the scintillating tip with a length L=1.0 mm, we modelled the effect of said misalignment on the optical power coupled into the POF. Figure 1c shows that for a sensor tip with a diameter D=0.5 mm (which matches the diameter of the POF), the coupled power almost linearly decreases with the amount of misalignment. Displacing the HDR-PMMA sensor by 0.05 mm lowers the coupled power from 0.275 to 0.243 a.u., which is a decrease of 11.4%, whilst shifting the LDR-PMMA sensor by 0.05 mm lowers the coupled power from 0.267 to 0.237 a.u., corresponding to a decrease of 11.2%. Small misalignments of the sensor tip may hence introduce a large variability from probe to probe. On the other hand, for a sensor tip with a diameter D=0.7 mm, the coupled optical power remains constant for displacements up to 0.1 mm. To allow for a ±0.1 mm alignment tolerance of the sensor tip with respect to the center of the POF core, whilst maximizing optical coupling within the space constraints and still fitting within the constraints of the Foley catheter as mentioned earlier, we therefore ultimately opted for a 0.7 mm-diameter cylindrical shaped sensor. In view of the fabrication technique used, we also accounted for a 2.2-degree demoulding angle, which transforms the cylindrical sensor tip into a truncated conical volume as illustrated in Figure 2, with little to no impact on the sensor performance. The presence of a demoulding angle is essential for successfully releasing the tips from the mould, resulting in dimensions of 0.7 mm for the long base, and 0.63 mm for the short base of the truncated cone. Additionally, and given that the optical properties of the two compound materials are similar (essentially in terms of attenuation), we chose to use identical designs for both the LDR-BT and HDR-BT sensor tips. This also makes sense in view of the fabrication, since this implies that the same fabrication mould can be used for manufacturing both types of sensor tips. The final shape of the scintillating tip is shown in Figure 2.
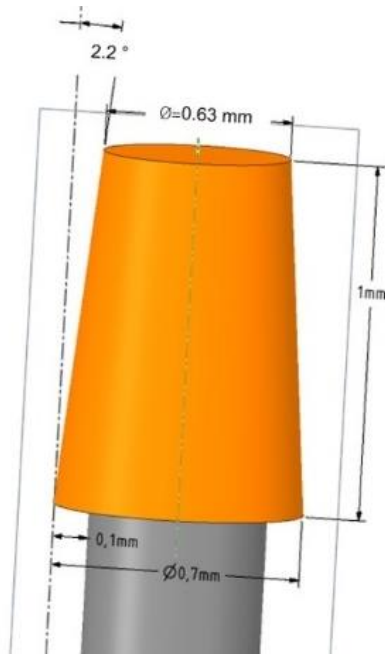
Figure 2. Illustration of the final LDR-BT and HDR-BT sensor tip design (orange) attached to the end facet of a 0.5 mm-diameter POF (grey).

2.4 Fabrication of the sensor tips.

Both the LDR and HDR scintillating tips have been fabricated by means of a custom two-step process using a Jenoptik HEX04 hot embossing and compression moulding machine. First, we manufactured substrates consisting of scintillating powder dispersed in PMMA, as described in detail in Section 2.1. The mixture of PMMA powder with inorganic scintillator powder was transformed into round, flat substrates with a custom mould fabricated from a copper-beryllium-cobalt alloy which was made by means of precision micro-milling. HDR-PMMA and LDR-PMMA substrates were manufactured at 120°C with a compression force of 10 kN. The substrates have a diameter of 15 mm with thickness ranging from around 0.5 mm to 4.7 mm depending on the mass of the mixture inserted into the mould cavity. Figure 1 of the Supplementary material shows photographs of the mould and some of the fabricated specimens. The typical cycle time to obtain one sample was ~10 minutes.

In the second step, this substrate is used for the manufacturing of multiple scintillating tips per cycle using a custom transfer moulding tool, of which the cross-section is illustrated in Figure 3. It consists of two main parts. The top part contains the cavity for the scintillating substrate (orange color) and the injection gates (pink color). The substrate is heated to 120°C and pushed downwards through the injection gates with a force of 10 kN generated by the Jenoptik HEX04 machine. This fills the 8 sensor tip cavities (dark green color) located below in the second part of the mould. Figure 3b shows the top view of the mould with the substrate (orange)

and the 8 injection gates (pink). Figure 3c shows a close-up of the injection gate (pink) and the scintillating tip cavity (green). With this approach, one substrate serves the transfer moulding of 8 tips for about 11 cycles, i.e. 1 substrate delivers about 88 sensor tips. The processing time of a single cycle to manufacture 8 tips takes around 15 minutes. This clearly indicates that the technology allows for small series fabrication. Note however that the transfer mould can easily be adapted to contain more than 8 cavities, enabling further upscaling of the manufacturing towards larger series.
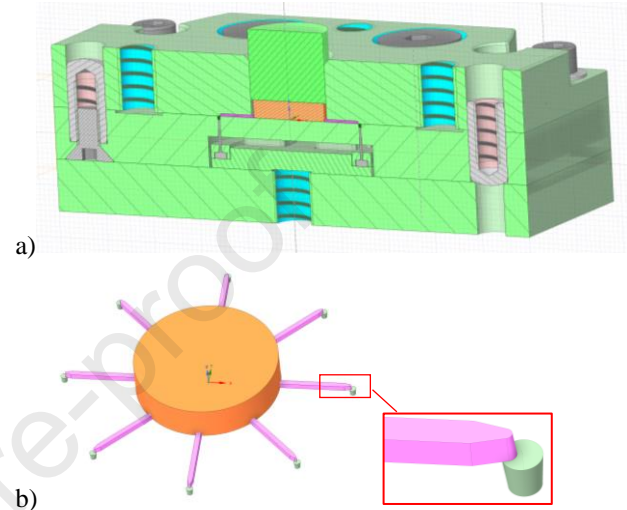

Figure 3. Technical drawing of a) a cross-section of the stacked mould structure used for the fabrication of the scintillating tips. The scintillating substrates are shown in orange; c) a close-up of the injection gate (pink) and the eventual scintillating tip (green). For scale: the orange cylinder has a diameter of 15 mm.

We manufactured a first batch of 17 LDR-BT and 21 HDR-BT probes for initial radiation tests and a second batch of 40 LDR-BT and 40 HDR-BT probes for examining the potential influence of the adhesive and protective tubing on the dosimetric response of the sensors. Finally, we manufactured a third batch of 59 LDR-BT and 60 HDR-BT, resulting in a series of 237 BT probes total. See Table 1 of the Supplementary Materials for an overview.

For the first batch, the HDR-BT tip length was around 992 $\pm$32 µm, which is deviating with 1% only from the design length of 1 mm; however, the long base diameter (614$\pm$37 µm) and top diameter (489$\pm$16 µm) of the truncated cone were respectively around 12% and 22% smaller than the design values. Similarly, the LDR-BT tip length was around 980 $\pm$52 µm which is a 2% deviation from the design; however, the long diameter (582$\pm$24 µm) and top base diameter (480$\pm$16 µm) of the truncated cone were respectively 17% and 24% smaller than the design values. The difference in top diameter of the truncated cone indicates that the demoulding angle of the tips deviated from around 2.2° to around 3.0° to 3.6°. Due to these unexpected smaller dimensions, the alignment tolerance of the sensor tips with respect to the POF decreased from $\pm$100 µm to $\pm$57 µm. The difference between the

measured tip dimensions and the design values stems from the dimensions of the cavities that were machined in our custom mould. This issue was solved by post-processing the mould such that said cavities were slightly enlarged.

The tips of the 2ⁿᵈ batch were then fabricated using said mould with corrected cavities. The average LDR-BT tip length was 1030 ± 25 µm, which is 3% larger than the design value. The bottom base has an average diameter of 690 ± 9 µm and the top base 576 ± 10 µm. These are only 1.5% and 8.6% smaller than the design values. The bottom diameter of the tips from the new batch is within the expected size range. The demoulding angle was kept at around 3.3° since re-drilling the cavities is not straightforward. The top diameter values of the 2ⁿᵈ batch and the 3ʳᵈ batch are therefore improved with respect to the 1ˢᵗ batch but do still not exactly match the design value. This, however, should not have a significant influence on the sensor tip performance given that the total volume of the tips is not affected much. Given the smaller standard deviation of the fabricated tips, we can also anticipate that the 2ⁿᵈ and 3ʳᵈ batch will feature less sample-to-sample variation.

2.5 Assembly of the brachytherapy probes.

We developed a dedicated procedure to align the scintillating tip with respect to the POF and to attach it to the POF end by means of UV-curable adhesive. To achieve this, the optical fiber was mounted in an FPH-DJ, Delrin-Jawed fiber chuck on a 3-axis translation stage, whilst the mould was mounted onto another precision 3-axis translation stage with the assistance of a custom-made fixture. To visualize the alignment procedure, we mounted a first USB microscope (Dino-Lite Edge 3.0) above the point of contact between the POF facet and the sensor tips in the moulding tool. Additionally, we positioned a second USB digital microscope (Dino-Lite Premier) sideways to the point of contact to provide a side view. A picture of the setup is shown in Figure 6 of the Supplementary Material. Prior to the alignment, the tips were pushed out of the mould cavities very slightly to facilitate their visualization. This was carried out by means of a dedicated ejection mechanism foreseen within the mould stack, which converts the torque applied to a lead screw into a force onto metal pins positioned directly below the tips (see also Figure 3a). To ensure the best alignment of the tip with the POF, we stripped a portion of the fiber jacket (over a length of around 2 cm) using a Micro-Strip™ stripping tool prior to inserting it in the fiber chuck.

To attach the tip to the POF facet, we manually applied a small amount of Norland Optical Adhesive (NOA) adhesive onto the POF facet, before precisely aligning the fiber in front of the sensor tip and then moving the fiber to achieve physical contact between POF and scintillating tip. To cure the NOA adhesive, we switched on a handheld UV light source (365 nm center wavelength, 200 mW emission power) from Polytec

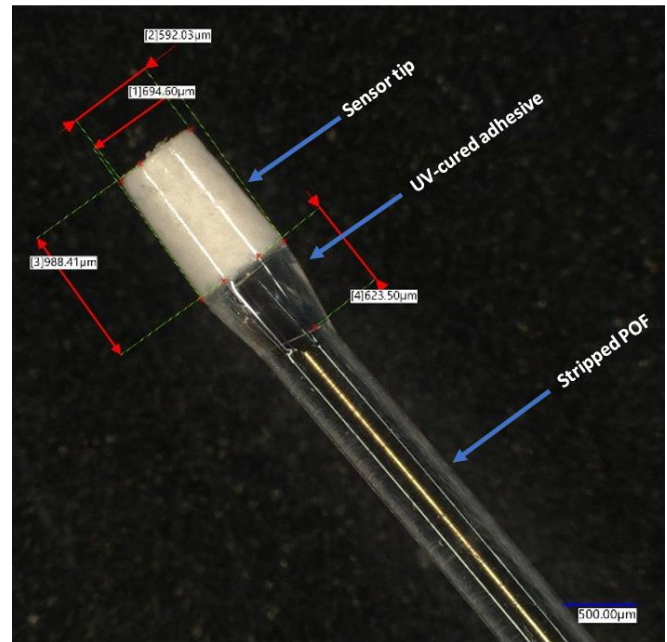GmbH positioned about 2-3 cm above the curing area for around 10 seconds.

Figure 4. Photograph of a sensor tip assembled to the POF. The dimensions of the assembly are indicated with red arrows.

Following the assembly of all the probes, we have measured their dimensions using a 4K High Accuracy Keyence VHX-7000 series Digital Microscope. An example of a microscope image of a probe consisting of scintillating tip attached to a POF is shown together with the dimensions in Figure 4.

To ensure sufficient robustness of the probes during handling and use, we applied two types of protective heat-shrink sleeves. The first was made from poly(vinylidene fluoride) and was acquired from PMG Company [17] whilst the second was made from polyolefin and was purchased from Cobalt Polymers. Both were colored black to prevent ambient light from reaching the scintillating tip and POF. The protective sleeves were fixed internally to the bare fiber and the sensor tip by means of UV-curing NOA adhesive, either NOA1665 or NOA65. To check if there is any influence on the measured signal from the adhesive or from the protective tubing, we fabricated 5 different sub-batches within the 2ⁿᵈ batch of LDR-BT and HDR-BT probes, each containing 8 sensors, leading to 40 sensors in total. Note that since the glue was applied manually, there is some variability in the volume applied. In the above description, the "standard amount of NOA adhesive" corresponds to the minimal amount of glue, applied to the cladding layer of the bare stripped fiber, which is required to attach the protective sleeve, whilst "an extra mount of NOA adhesive" corresponds to 3-4 times the minimal amount of glue. The 3ʳᵈ batch of LDR-BT and HDR-BT probes was equipped with a black Polytetrafluoroethylene (PTFE) tube, which enhances the durability and robustness.

The PTFE tube was internally glued to the bare portion of the POF with UV-curable NOA68 adhesive, which has a lower refractive index n=1.54 and features improved adhesion to PTFE compared to NOA1665. An overview of the different manufactured batches and the protection that was applied to the probes is shown in Table 2.

Table 2. Overview of the fabricated LDR-BT and HDR-BT probes.

Batch no.	Sub-batch no.	Protective Tubing	Adhesive
1st batch	2.X	None/ unstripped fiber	----
	3.X	None/ stripped fiber	----
	4.X	PMG MT02	NOA 1665 n=1.665, standard
2nd batch	5.X	None/ stripped fiber	----
	6.X	PMG MT02	NOA 1665 n=1.665, standard
	7.X	PMG MT02	NOA 1665 n=1.665, extra
	8.X	PMG MT02	NOA 65 n=1.52
	9.X	Cobalt Polymers X2 034	NOA1665
3rd batch	c1-c8	PTFE	NOA68, n=1.54

2.6 Dosimetric response of the LDR-BT probes

The LDR-BT optical fiber-based dosimeters were tested at Blackrock Health Galway Clinic, Ireland using an ^{125}I brachytherapy ionizing radiation source.

The photon counting detector system employed in this work is provided as part of the CAEN SP5600E Educational Photon Kit. The components employed were the CAEN SP5600 power supply and amplification unit (PSAU), the CAEN DT5720A desktop digitizer (required only for activation of the CAEN control software), and a Thermo Electrically (TE) Cooled Hamamatsu SiPM that has a photosensitive area of 1.3 x 1.3 mm^2, a pixel pitch of 50 μm, 667 pixels, and a Dark Count Rate (DCR) of approximately 2.5 kHz at the 0.5 photo-electron threshold level. The measured parameter of interest was the photon count rate, which is the signal generated within the SiPM in excess of the dark count rate, due to the presence of a scintillation signal.

Radiation characterization of LDR-BT probes was performed using a commercial water phantom system PTW MP3-XS (PTW, Freiburg, Germany), integrated with custom 3D-printed components, allowing for a more precise evaluation of the sensor performance. Utilizing a water phantom filled with sterilized water facilitates the acquisition of clinical measurements in a standardized, replicable, and dosimetrically precise setting, thereby ensuring accurate results. The in-house manufactured water phantom system's primary components consisted of a support frame, a sensor holder, and a source holder. All 3D-printed components were fabricated using a Stratasys Objet Connex500 3D Printer, with a printing accuracy of ~ 64 μm. The material employed was a PolyJet^{TM} material (model MED610), with a density of 1.17 – 1.18 g/cm^{-3}. As illustrated in Figure 5, the support frame employs a "T-junction" design, securing the upper part of the water phantom. Extending from the support frame is a 100 mm long "guide tube," which facilitates the delivery of a 3D-printed sensor holder into the water phantom. The support frame is securely anchored on three sides of the tank, ensuring consistent positioning within the water phantom for each setup. The 3D-printed sensor holder is designed to incorporate a channel through which a plastic needle is inserted, housing the LDR-BT sensor. Both the guide tube and sensor holder are engineered to maintain precise alignment of the plastic needle, ensuring that the sensor is positioned in parallel orientation with respect to the ^{125}I seed. Finally, the 3D-printed source holder is designed to fit seamlessly into a TRUFIX "Roos Electron Chamber" holder. Consequently, it can be mounted on the mechanical stage of the water phantom, enabling precise measurements. The ^{125}I seed is positioned within a channel near the tip of the source holder component, with the channel's dimensions matching that of the seed.
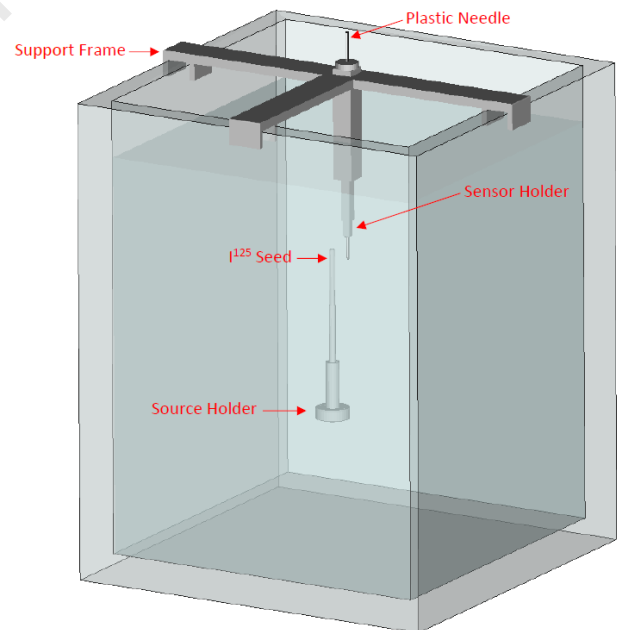

Figure 5. Illustration of the water phantom system for characterizing the LDR-BT probes, including different 3D-printed components.

The main alteration to the experimental setup within the water phantom, in comparison to that previously reported in [11] involves swapping the positions of the sensor and source, i.e., the sensor is now introduced through the support stage at the top of the water phantom, while the source is mounted on the mechanical stage. This configuration offers a notable advantage as it greatly simplifies the exchange of optical fiber

sensors, which is crucial when one wants to compare the different fiber sensing probes with each other.

Figure 7 of the Supplementary Material shows the experimental setup for evaluating the dosimetric response of the LDR-BT sensor probes. The optical fiber sensor exits the above-mentioned water phantom system and is connected to a TE Cooled SiPM via an optical coupling system obtained from ThorLabs, Inc., which consists of an aspheric lens (model C340TMD-B) and a focuser (model F230SMA-A). A comprehensive report of the rationale behind the utilization of this coupling system and its detailed description can be found in [19]. The output of the TE-Cooled module is connected to the input of the PSAU, which is employed only as a frequency counter for the purposes of this work. The PSAU and digitizer are interfaced to a laptop computer via USB 2.0 connections, allowing for readout and analysis of the measurement data.

The ^{125}I seed was surrounded with ≥ 10 cm of sterile water in all directions, ensuring consistent and accurate scattering conditions and allowing for precise dosimetric measurements to be obtained. Initially, the center of the sensor was aligned with the center of the radiation source visually, defining a preliminary "null point" (i.e., the origin of the coordinate system). This in turn defined the position of the sensor relative to the ^{125}I seed. Fine-tuning of the preliminary "null point" can then be performed radiologically. That is to say, when the sensor and the ^{125}I source are positioned parallel to one another, assuming correct alignment, we would expect the scintillation signal detected at equal distances, on opposing sides of the source, to be equivalent (since the dose-rate from the source is cylindrically symmetrical). Fine-tuning the position of the null point, in 0.1 mm increments, is performed until this condition is met, within measurement uncertainty. The Hamamatsu TE-Cooled SiPM employed in this work was a stand-alone module, of which the characterization for brachytherapy purposes can be found in [18]. Therefore, bias voltage (V), gain (dB), or discriminator threshold (p.e. or mV) settings within the CAEN control software were not configured. However, since the SP5600 PSAU was used as a frequency counter, counting parameters needed to be defined. Specifically, the gate-width was set to 10 ms, and the number of points to average for each mean value calculated was set to 10. Defining the counting parameters in this manner resulted in a photon count rate data point being generated every 100 ms (10 ms x 10). While this might suggest a sampling frequency of 10 Hz, there was a data transfer reduction to 2 Hz using the CAEN system. The analysis of the data generated by CAEN using the CAEN control software involved several steps: importing the raw dataset, subtracting the mean DCR value from the raw counts to provide a measure of the photon count rate, and finally calculating both the mean photon count rate signal and the standard deviation thereof for each position.

2.7 Dosimetric response of the HDR-BT probes

The HDR-BT optical fiber-based dosimeters were tested at Queen's University Belfast, UK, using an ^{192}Ir brachytherapy ionizing radiation source, delivered from an Elekta Flexitron afterloader.

The radiation tests on HDR-BT probes have been carried out with both water and Perspex® phantoms setup illustrated in Figure 8 of the Supplementary Material. Where an effective dwell time is specified, this is the dwell time that is weighted using the measured air kerma strength at the time compared to the reference of 40,000 cGy cm²/h air kerma strength. The photon counting kit used for HDR-BT radiation characterization was the developed ORIGIN 16-channel fiber sensor system, of which the operational description was reported in [20]. This consists of an array of sixteen 1.0 x 1.0 mm² Ketek SiPMs, with a typical DCR of 125 kHz when operated at the 0.5 photo-electron level [20].

The 16-channel system output is processed using a CAEN FERS-5200 front-end readout system, which is connected to a laptop and controlled using CAEN JANUS digital acquisition software. This system enables a maximum photon count rate of 20 MHz to be measured.
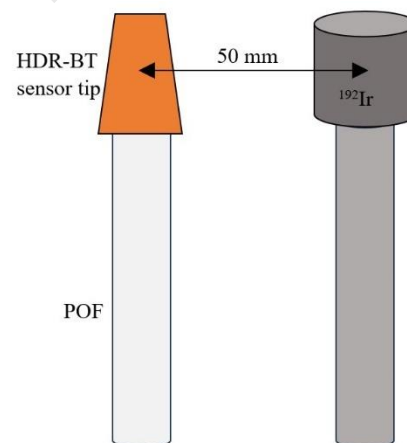

Figure 6. Schematic illustration of the fundamental physical setup used to characterize all of the HDR-BT sensors. The ^{192}Ir source was set to dwell at a distance of 50 mm from the sensor tip.

To assess the radiation response of the HDR-BT probes, the sensor batches were tested in a water phantom tank adapted to position 16 BT probes concentrically at various source-probe distances. In order to minimize the influence of positional error on comparative measurements, the analysis focuses on the photon count rate at a distance of 50 mm from the ^{192}Ir source, as shown in Figure 6. A flat Perspex® plate with linear grooves at 1 cm separation was used for all measurements, following the 1st batch of HDR-BT probes. Both the ^{192}Ir source and HDR-BT probes were inserted into plastic brachytherapy needles that snugly fit into the grooves, offering improved optical fiber positional accuracy. An additional 5 cm-thick Solid Water® block was placed on top

to account for backscatter. This setup was characterized by conducting repeated measurements using a single probe from the HDR-BT batch. Additionally, a single SiPM was used to eliminate variations in measurements arising from different SiPM-optical fiber combinations. The measurement error in the Perspex® phantom at a 50 mm source-to-probe distance is 1.3%, taking into account statistics, setup reproducibility, and positional uncertainty.

3. Results and discussion

3.1 Dosimetric response of the LDR-BT probes.

Figure 7a presents a box and whisker plot of the photon count rate obtained for 17 sensor probes, with the sensors separated into two batches (9 fibers 2.X which were "unstripped" and 8 fibers 4.X which were "stripped" of their protective jacket and subsequently sealed with black heat-shrink tubing PMG MT02). Two features are clearly visible in Figure 7a. Firstly, the variability for the stripped fibers ($\sigma^2 = 143.1$ kHz^2) is greater than that of the unstripped fibers ($\sigma^2 = 15.4$ kHz^2). Secondly, the stripped fibers have a much larger mean scintillation signal ($\bar{x} = 66.3$ kHz) compared to the unstripped fibers ($\bar{x} = 46.4$ kHz). It is worth noting at this point, that the DCR remained constant for both sensor batches at 2.4 kHz. A Welch's t-test was performed to determine if there is a statistically significant difference in the photon count rate values measured for the unstripped and stripped sensor probes. A statistically significant difference ($\alpha = 0.05$) in the mean photon count rate values ($t = -4.512$, $p = 0.002$) was found between the two. Because of this result, we decided from then on to assemble the sensor tip to a partially stripped fiber section which most likely improved the positioning of the senor tip to the POF end facet.

Figure 7b shows the average responses and their variations for the 5 configurations from the 2nd batch (see Table 2). Overall, the mean photon count rate signal remained relatively consistent for sub-batches 5.X, 6.X, and 7.X, while the average photon count rate is lower for sub-batch 8.X, since it uses an adhesive with a lower refractive index, which is detrimental for the light coupling into the POF.

After dismantling and re-assembling the water phantom setup, the photon count rate measurement was repeated with a different ^{125}I source, and with a 10 mm source-to-sensor distance to verify the reliability and reproducibility of the setup. The results (shown in Figure 8 of the Supplementary Material) underscore the good reliability of the measurement setup and the repeatability of the results.

The 3rd batch of 59 LDR-BT probes were assembled using unstripped POF with PTFE black tubing covering the length of the bare fiber section (~1.5 cm) and the sensor tip. For this batch, we conducted the identification of the sensor tips and their locations within one of the 8 cavities (labelled c1 to c8) within the transfer moulding tool. Additionally, we evaluated

the statistics concerning the geometrical features of the scintillating tips to identify potential causes for variations in the scintillation signals coupled into the POFs.
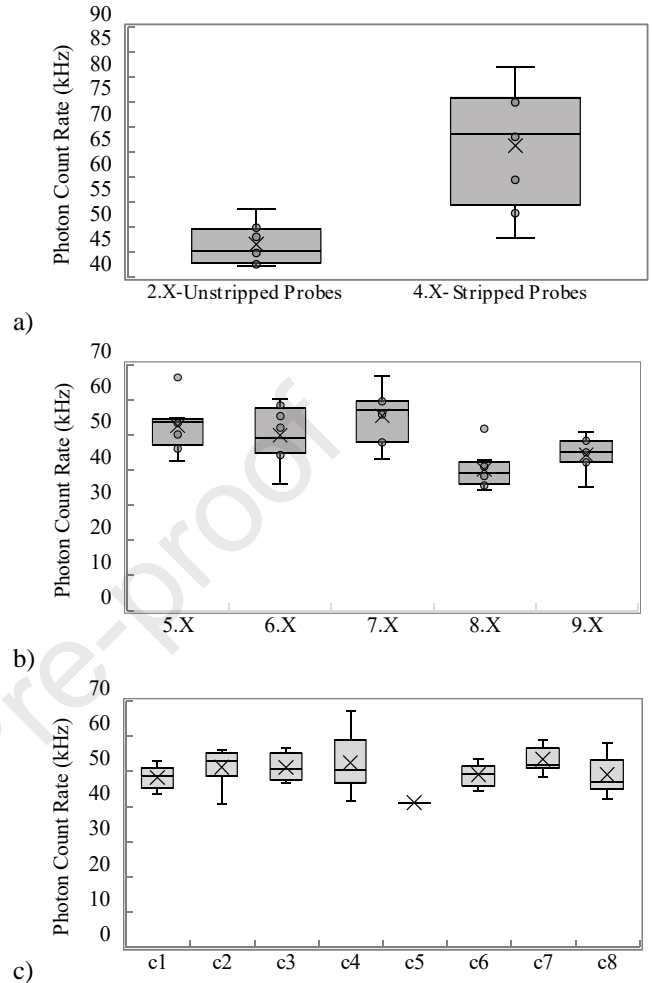
a)

b)

c)

Figure 7. Box and whisker plots of the measured photon count rate, a) comparing 17 LDR-BT sensor probes from the 1st batch employing two fabrication configurations (see Table 2); b) for the 5 types of 2nd batch LDR-BT probes at 5 mm-distance from the ^{125}I source; c) for the 3rd batch of LDR-BT probes originating from one of eight cavities (c1-c8) in the mould, at 5 mm-distance from the ^{125}I source. Note that only one probe from c5 was investigated, hence this measurement can be neglected.

The photon count rate data obtained from this batch, shown in Figure 7c, did not reveal any specific increase in the radiation signal for particular groups of sensor tips originating from distinct cavities in the transfer moulding tool. The analysis of sensor tips located within various cavities did not demonstrate any consistent trend indicating either higher or lower photon count rates, suggesting homogeneity in the composition of the fabricated sensor tips. Furthermore, concerning the calculated average sensor tip volumes, the radiation experiments indicated that neither larger volume sensor tips nor smaller volume sensor tips exhibited higher or lower photon count rates.
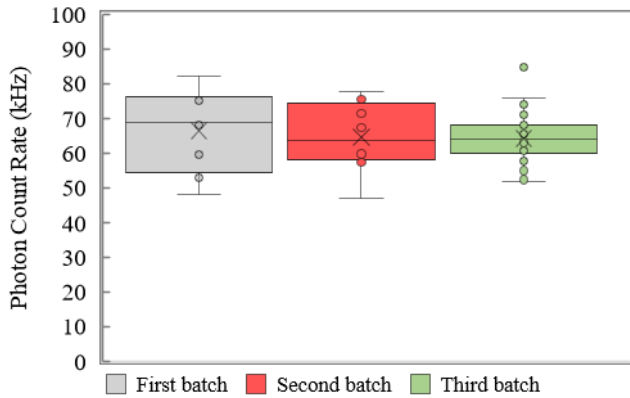
Figure 8. Box and whisker plot of the measured photon count rate, comparing LDR-BT sensor probes employing equivalent fabrication configurations from three batches.
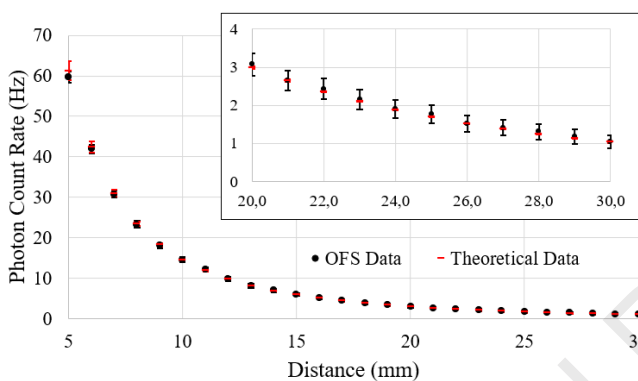

Figure 9. Photon count rate fall-off as a function of source-to-probe distance with a relative comparison of the measured data (black dots) to the theoretical expectation (red dashes). Inset: close-up on the distance range from 20 to 30 mm.

Furthermore, if we compare the probes from all three batches employing equivalent fabrication methods in terms of the protective tubing and applied NOA1665 glue, specifically the stripped probes from the first batch (4.X, Figure 7a) with the 6.X sub-batch from the 2nd batch of 40 probes sensors (Figure 7b), with the sensors from the 3rd batch (Figure 7c), we can see in Figure 8 that there is consistency in the magnitude of the mean photon count rates measured for all the probes, after correction for the different source activities. Additionally, the 3rd batch presents less variability in the measured photon count rates. The response of LDR-BT sensors produced in each batch has been shown to be consistent when the same fabrication method is employed. Furthermore, the uniformity of sensor responses within a given batch has demonstrated improvement with each successive batch. Nevertheless, the uniformity of the sensor response is not such that a single calibration factor can be applied to all sensors within a given batch. Consequently, individual calibration is necessary for each sensor. Therefore, when assessing the sufficiency of this approach for clinical applications, the limiting factor becomes the magnitude of the response and its adequacy in ensuring accurate results (i.e.,

low statistical uncertainty) within the required integration time (< 1 s).

For the purpose of evaluating the fall-off of the photon count rate as a function of distance from the probe, we used the following approach. First, an ^{125}I source was inserted into the source holder, whilst the probe was inserted into a plastic needle. Second, we initially aligned the source with the probe, and then we moved the source more than 10 cm away from the probe for a DCR measurement (with an integration time set to 30 s). Next, the source was moved to a distance of 5 mm from the probe, the alignment was verified, and the photon count rate was measured at distances of 5 to 30 mm in increments of 1 mm (again with integration time offset of 30 s). The last step was repeated 5 times to allow for averaging the photon count rate measurements, to minimize the effect of the uncertainty on the source position (reproducibility of the mechanical positioning is ±0.1 mm). Figure 9 shows the photon count rate fall-off along the transverse axis as a function of distance from the source. It is consistent with theoretical expectations and is independent of the magnitude of the scintillation signal within statistical uncertainty. The theoretical fall-off in dose rate data was calculated by the Carleton Laboratory for Radiotherapy Physics (CLRP) using the egs_brachy Monte Carlo software, as part of their TG-43 parameter database (specifically designed for the AgX100 ^{125}I seed). This finding indicates that that there is no need for an "energy correction" to account for changes in the energy spectra based on the distance from the source and the use of high-density (non-tissue equivalent) inorganic scintillator material in LDR-BT applications.

Kirisits et al. conducted an analysis of uncertainties associated with ^{125}I LDR brachytherapy, reporting a total dosimetric uncertainty of 11% [21]. To assess our LDR-BT probes within this uncertainty framework, we can examine the standard error (with a confidence level k=3). At a 5 mm-distance from the source, LDR-BT probes exhibit a standard error of 2.2%, which increases to 16.2% at 30 mm. This highlights the importance of precise positioning of the LDR-BT probes during treatment, as well as careful consideration of the integration time and sampling frequency when determining the statistical uncertainty for the final LDR-BT clinical system.

3.2 Dosimetric response of the HDR-BT probes.

The 1st batch, consisting of 21 fibers, allowed us to compare the photon count rate from HDR-BT probes prepared from stripped and unstripped optical fibers (see Table 2). The results in Figure 10a demonstrate that the highest photon count rate is achieved for the 4.X probes, with a relatively greater σ difference in photon count rate between probes from the same sub-batch 4.X (σ = 100.1 kHz) and 2.X (σ = 59.1 kHz). Figure 10b presents the photon count rate dataset for the 2nd batch of HDR-BT probes, which were assembled using various configurations (see Table 2).
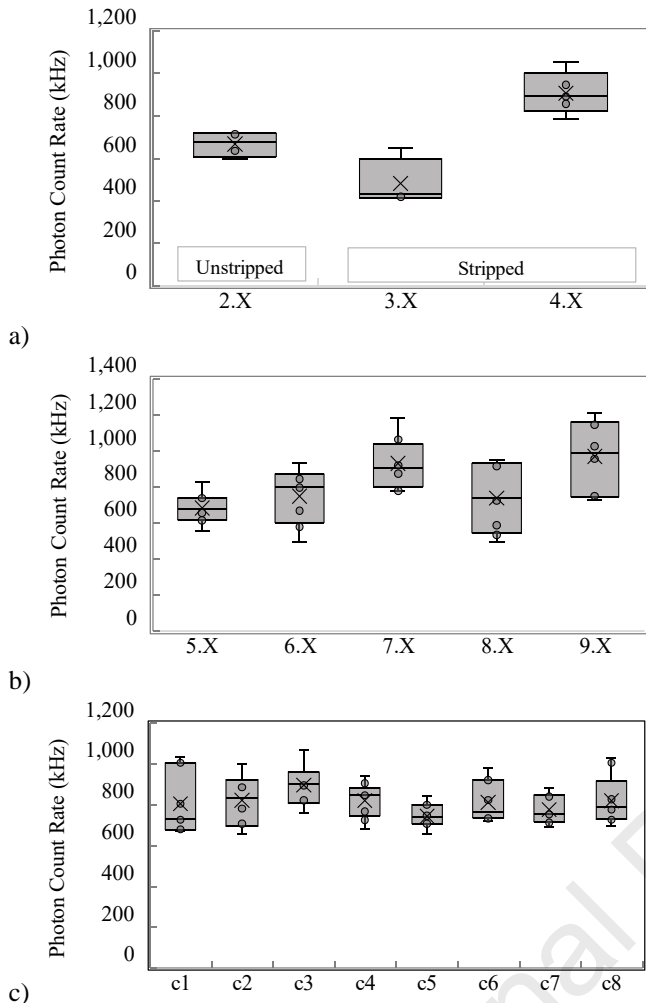
Figure 10. Box and whisker plot of the photon count rate measured a) for the 1st batch of unstripped and stripped HDR-BT probes; for the 2nd batch of HDR-BT probes, comparing probes in 5 different protective configurations, at 50 mm-distance from the ^{192}Ir source; c) for the 3rd batch of HDR-BT probes, comparing the probes originating from one of eight cavities (c1-c8) the mould at 50 mm-distance from the ^{192}Ir source

The highest photon count rate is observed in HDR-BT sensors of type 9.X (covered with X2 034 Polyolefin-based shrink tubing supplied by Cobalt Polymer). Interestingly, this trend is not observed for LDR-BT sensors covered with that particular tubing. However, the HDR-BT of type 8.X featured a decrease in photon count rate, in line with the observations for the LDR-BT probes, due to the lower refractive index of the glue and the consequently lower coupling of the scintillation signal into the POF. Applying an extra amount of NOA1655 in types 7.X enhanced the photon count rate, just like for the LDR-BT probes (see Figure 7b). When tracking mechanically damaged sensors in the batch, it was noted that PMG MT02 offered superior protection compared to Cobalt Polymer, since 2 out of 8 Cobalt Polymer-covered probes in this batch were damaged, whereas no other breakages were recorded.

The 3rd HDR-BT batch was uniquely numbered according to the respective mould cavity in which the sensor tip was made. A single-factor Analysis of Variance (ANOVA) test was performed on the measurements shown in Figure 10c, yielding a p-value of 0.42, clearly indicating a lack of statistical significance in the differences observed among HDR-BT probes with scintillating sensor tips originating from distinct mould cavities. Given the substantial batch size of 60 probes, all sharing an identical configuration assembly, individual probe outputs were evaluated against specific physical characteristics of the sensor tips, including length and volume. Table 2 of the Supplementary Material provides the Pearson correlation coefficients for each of these characteristics. The analysis of HDR-BT probe characteristics within the 3rd batch revealed no discernible correlation between the geometrical properties of the probes and their photon count rate output.

In their studies, Kirisits et al. conducted an analysis of uncertainties associated with HDR-BT treatments [21]. They determined that when employing a ^{192}Ir vaginal cylinder applicator, the composite uncertainty amounted to 8%, while for ^{192}Ir prostate treatment, it was 5%. Cervical cancer treated with image guided intracavitary brachytherapy also had an uncertainty of 5% when delivered in four fractions. In our case, when considering a typical photon count rate at 10 cm away from the radiation source, which represents the farthest expected point for HDR-BT probe utilization during treatment, the standard deviation in counts was approximately 1.7%. This is further reduced to 0.2% when measurements are taken at a distance of 1 cm from the source. These statistical uncertainties represent a small contribution to the uncertainty budget for the probes that will permit deviations in treatment delivery to be detected in real time and for the treatment course. The 3rd and final batch of HDR-BT probes were found to be acceptable using the statistical uncertainty in a measurement as criteria.

The typical DCR defined by the SiPM datasheet is 125,000 Hz. Using the definition of minimum detectable signal in photon counting of Bronzi et al. [22], the minimum detectable using our HDR system is 1067 Hz [20]. A typical HDR-BT probe measures a photon count rate of 409k Hz when positioned at 5 cm from an ^{192}Ir source, receiving a dose rate of 2.36 mGy/s. Using average probe characteristics, this equates the minimum detectable signal to a dose rate of 6.14 µGy/s, to measure such a dose rate the probe must be irradiated by the source from a distance of approximately 1 meter, a significant distance from the body with no clinical significance.

Table 3. Comparison with state-of-the-art HDR-BT dosimetry

Reference	Scintillator/ Detector	Readout System	Source	Statistical Uncertainty	Statistical Uncertainty Method
[24]	Y2O3:Eu + 4YVO4:Eu	Charge-coupled device (CCD)	Iridium-192	0.3% at 2 cm	Standard Deviation of 10 repeat measurements without source retraction
[25]	BCF-12	Photomultiplier	50 kVp X-ray Tube	0.1 to 1.3%	Irradiations using an X-ray source of a fixed detector. Standard deviation of 10 second measurements over a 300 second period. Repeated six times
[26]	PTW 9112 Diode Array	Electrometer	Iridium-192	0.3% at 8 cm	Standard deviation of signal during repeated 5-minute measurements
[27]	ZnSe:O	Photodiode	Iridium-192	0.25% at 2 cm	Calibration irradiation, repeated 189 times
[28]	Zn(Cd)S:Ag	Silicon Single Photon Avalanche Photodiode	Iridium-192	0.03% at 2 cm	Signal standard deviation with a fixed dwell position
This work	Y2O3:Eu + 4YVO4:Eu	SiPM	Iridium-192	0.57% at 2 cm	Standard deviation of 100 measurements without source retraction

With the determination of calibration factors in advance of the use of the sensors in-vivo, point dose rates can be obtained at the instant of measurement. A sampling rate of 10 Hz along with the development of software to convert photon count rate measurements to dose rate will deliver a sufficient frequency of measurement in the application of HDR brachytherapy, where a sampling rate of 5 Hz is required to identify clinically relevant errors [23].

Table 3 shows an overview of the state-of-the-art fiber-based dosimetry for HDR brachytherapy. A combination of scintillation material paired with a charge-coupled device (CCD) camera offered a similarly low statistical uncertainty of 0.3% at 2 cm [24]. This configuration was aided by a reflective material on the tip to enhance signal intensity and a 1 mm-diameter optical fiber [24]. A study using a plastic scintillator, namely BCF-12, intended for brachytherapy verification was shown to have a similar range of noise when irradiated using a lab x-ray source at high dose rates [25]. The use of a low-noise photomultiplier tube in this study and when compared to the HDR-BT probes coupled to an SiPM in this paper reinforces the suitability of this configuration, with similar levels of noise being reported in other studies using an inorganic scintillator [27]. The lowest statistical uncertainties were reported by a study involving a small volume zinc sulfide-based scintillator intended for brachytherapy dosimetry, this optical fiber sensor offered great sensitivity due in part to it being coupled to a temperature-controlled photon counter [28]. There are few examples of commercial systems for brachytherapy dosimetry. The PTW-9112 system has a diode array coupled to an electrometer which has been

characterized to have a statistical uncertainty of 0.3% at 8 cm [26]. This is low relative to our HDR-BT probes at this distance, however other uncertainties exist within this system that negate the low statistical uncertainty [26], [29].

4. Conclusion

In conclusion, we demonstrate the fabrication of a series of 237 HDR-BT and LDR-BT sensor probes with their initial testing as an ionizing radiation sensor performed in water phantoms. Our main objective was to optimize the design of the sensor tips for HDR-BT and LDR-BT to enable low-cost, and high-throughput manufacturing of the tips by making their design compatible with replication techniques such as compression and transfer moulding. Due to the very similar optical properties of both HDR and LDR scintillating materials, we obtained almost identical optical coupling properties, and as a result the final design of sensor tips is the same for the HDR-BT and LDR-BT probes. This means that we were able to use the same mould for the fabrication of both the HDR-BT and LDR-BT probes. We developed a custom transfer moulding process in which we first manufactured blank substrates consisting of a mixture of PMMA and respectively LDR or HDR scintillator. Subsequently, these substrates were employed in a second transfer moulding step to create eight sensor tips simultaneously within a single moulding run. We then performed the assembly of the sensor tips to the polymer optical fibers using UV-curable adhesive, which was followed by covering of the BT probes in various configurations with different types of protective tubings. To this end, we mostly used NOA1665 adhesive, which after

curing has a refractive index n=1.665, close to the refractive index of the scintillator materials (which is respectively n=1.81 for HDR-BT, and n=2.3 for LDR-BT). This resulted in more efficient light coupling and subsequently an increased photon count rate signal compared to NOA65 adhesive, which has a lower refractive index of n=1.52.

From our dosimetric response measurements, we observe that the mean photon count rate remained relatively consistent among HDR-BT and LDR-BT sub-batches, but some variability indicated the need for further investigations. The response of LDR-BT and HDR-BT sensors within each of the three fabrication batches has consistently exhibited conformity when the same fabrication and assembly method was employed. However, individual sensor calibration remains necessary since the uniformity is not to the extent that a single calibration factor can be universally applied to all sensors within a particular batch.

In essence, this paper contributes to the field by presenting a comprehensive exploration of optical fiber dosimetry tailored for brachytherapy, showcasing a harmonious fusion of precision engineering and medical innovation. We show that our dosimetry experiments in water phantoms exhibit good consistency in the magnitude of the average photon count rate for both the HDR-BT and LDR-BT sensors and that the photon count rate was not significantly affected by small variations in sensor tip composition and geometry, nor assembly tolerances. Whilst individual calibration remains necessary, the proposed dosimeters therefore show great potential for in-vivo dosimetry for brachytherapy, the more so because we have shown that they can manufactured in large series in a repeatable way.

Acknowledgements

Competing interests

The authors declare that they have no competing interests.

References

[1] Baskar, R., Lee, K.A., Yeo, R., Yeoh, K.W. (2012). Cancer andradiation therapy: Current advances and future directions. *Int. J. Med. Sci.*, 9(3), 193-199, https://doi:10.7150/ijms.3635.

[2] Podgorsak, E.B. (2005). Radiation oncology physics: a handbook for teachers and students. Vienna, Austria: International Atomic Energy Agency, p. 454.

[3] Liberman, D., Mehus, B., & Elliott, S. P. (2014). Urinary adverse effects of pelvic radiotherapy. *Translational Andrology and Urology*, 3(2), 186–195. https://doi.org/10.3978/j.issn.2223-4683.2014.04.01

[4] Wosniok, A. and Krebber, K.: Distributed fiber optic radiation sensors, *Saf. Nucl. Waste Disposal*, 1, 15–16, https://doi.org/10.5194/sand-1-15-2021, 2021.

[5] Zhang, J., Xiang, Y., Wang, C., Chen, Y., Tjin, S.C., Wei, L. (2022) Recent Advances in Optical Fiber Enabled Radiation Sensors. *Sensors* 22, 1126. https://doi.org/10.3390/s22031126

[6] Ding, L., Wu, Q., Wang, Q. et al. (2020) Advances on inorganic scintillator-based optic fiber dosimeters. *EJNMMI Phys* 7, 60. https://doi.org/10.1186/s40658-020-00327-6

[7] Lambert, J., McKenzie, D. R., Law, S., Elsey, J., & Suchowerska, N. (2006). A plastic scintillation dosimeter for high dose rate brachytherapy. *Physics in Medicine and Biology*, 51(21), 5505–5516. https://doi.org/10.1088/0031-9155/51/21/008

[8] Penner, C., Woulfe, P., Stoeber, B., Duzenli, C., O'Keeffe, S., & Hoehr, C. (2019). Novel optical fibre-based sensors for neutron and proton beams. *Proceedings of IEEE Sensors*, 2019-Octob, 1–4. https://doi.org/10.1109/SENSORS43011.2019.8956683

[9] Therriault-Proulx, F., Beddar, S., & Beaulieu, L. (2013). On the use of a single-fiber multipoint plastic scintillation detector for 192Ir high-dose-rate brachytherapy. *Medical Physics*, 40(6), 1–10. https://doi.org/10.1118/1.4803510

[10] Woulfe, P., Sullivan, F. J., Byrne, L., Doyle, A. J., Kam, W., Martyn, M., & O'Keeffe, S. (2021). Optical fibre based real-time measurements during an LDR prostate brachytherapy implant simulation: using a 3D printed anthropomorphic phantom. *Scientific Reports*, 11(1), 1–8. https://doi.org/10.1038/s41598-021-90880-6

[11] Martyn, M., Kam, W., Woulfe, P., & O'Keeffe, S. (2023). Water Phantom Characterization of a Novel Optical Fiber Sensor for LDR Brachytherapy. *IEEE Sensors Journal*, 23(2), 1146–1156. https://doi.org/10.1109/JSEN.2022.3225007

[12] Phosphor Technology Ltd. (n.d.). *PHOSPHOR TECHNOLOGY LTD*. Retrieved December 5, 2022, from https://www.phosphor-technology.com/

[13] Beddar, A. S., Mackie, T. R., & Attix, F. H. (1992). Cerenkov light generated in optical fibres and other light pipes irradiated by electron beams. *Physics in Medicine & Biology*, 37(4), 925. https://doi.org/10.1088/0031-9155/37/4/007

[14] Therriault-Proulx, F., Beaulieu, L., Archambault, L., & Beddar, S. (2013). On the nature of the light produced within PMMA optical light guides in scintillation fiber-optic dosimetry. *Physics in Medicine & Biology*, 58(7), 2073. https://doi.org/10.1088/0031-9155/58/7/2073

[15] Cometti, S., Gierej, A., Giaz, A., Lomazzi, S., Baghdasaryan, T., Van Erps, J., Berghmans, F., Santoro, R., Caccia, M., & O'Keeffe, S. (2022). Characterization of scintillating materials in use for brachytherapy fiber based dosimeters. *Nucl. Instr. Meth. in Phys. Res. Sect. A: Accelerators, Spectrometers, Detectors and Associated Equipment*, 1042, 167083. https://doi.org/10.1016/j.nima.2022.167083

[16] Polyanskiy, M. N. (n.d.). *Refractive index database*. Https://Refractiveindex.Info. Retrieved December 9,

2022, from
https://refractiveindex.info/?shelf=organic&book=poly(methyl_methacrylate)&page=Sultanova

[17] PMGCompany. (n.d.). *PMG COMPANY*. Retrieved March 31, 2023, from https://www.pmgcompanyonline.com/

[18] Caccia, M., Giaz, A., Galoppo, M., Santoro, R., Martyn, M., Bianchi, C., Novario, R., Woulfe, P., O'Keeffe, S. (2024). Characterisation of a Silicon Photomultiplier Based Oncological Brachytherapy Fibre Dosimeter. *Sensors*, 24, 910. https://doi.org/10.3390/s24030910

[19] Martyn, M., Kam, W., Giaz, A., Cometti, S., Santoro, R., Woulfe, P., Caccia, M., & O'Keeffe, S. (2022). Evaluation of a novel inorganic scintillator for applications in low dose rate (LDR) brachytherapy using both TE-cooled and room temperature silicon photomultipliers (SiPMs). In F. Berghmans & I. Zergioti (Eds.), *Optical Sensing and Detection VII* (Vol. 12139, p. 121390K). SPIE. https://doi.org/10.1117/12.2621268

[20] Giaz, A., Galoppo, M., Ampilogov, N., Cometti, S., Hanly, J., Houlihan, O., Kam, W., Martyn, M., Mc. Laughlin, O., Santoro, R., Workman, G., Caccia, M., & O'Keeffe, S. (2023). ORIGIN, an EU project targeting real-time 3D dose imaging and source localization in brachytherapy: Commissioning and first results of a 16-sensor prototype. *Nucl. Instr. Meth. in Phys. Res., Sect. A: Accelerators, Spectrometers, Detectors and Associated Equipment*, 1048, 167999. https://doi.org/10.1016/j.nima.2022.167999

[21] Kirisits, C., Rivard, M. J., Baltas, D., Ballester, F., De Brabandere, M., van der Laarse, R., Niatsetski, Y., Papagiannis, P., Hellebust, T. P., Perez-Calatayud, J., Tanderup, K., Venselaar, J. L. M., & Siebert, F.-A. (2014). Review of clinical brachytherapy uncertainties: analysis guidelines of GEC-ESTRO and the AAPM. *Radiotherapy and Oncology : Journal of the European Society for Therapeutic Radiology and Oncology*, *110*(1), 199–212. https://doi.org/10.1016/j.radonc.2013.11.002

[22] Bronzi, D., Villa, F., Tisa, S., Tosi, A., Zappa, F. (2016) SPAD Figures of Merit for Photon-Counting, Photon-Timing, and Imaging Applications: A Review, *IEEE Sensors Journal* 16(1), pp. 3-12, https://doi.org/10.1109/JSEN.2015.2483565

[23] Johansen, J.G., Kertzscher, G., Jørgensen, E.B., Rylander, S., Bentzen, L., Hokland, S.B., Søndergaard, C.S., With, A.K.M., Buus, S., Tanderup, K. (2019) Dwell time verification in brachytherapy based on time resolved in vivo dosimetry. *Phys Med.* 60:156-161. https://doi.org/10.1016/j.ejmp.2019.03.031

[24] Kertzscher, G., Beddar, S. (2019) Inorganic scintillation detectors for 192Ir brachytherapy. *Phys Med Biol.*, 64(22):225018. https://doi.org/10.1088/1361-6560/ab421f

[25] Georgi, P., Kertzscher, G., Nyvang, L., Šolc, J., Schneider, T., Tanderup, K., Johansen, JG. (2022) Toward 3D dose verification of an electronic brachytherapy source with a plastic scintillation detector. *Med Phys.* 49(5):3432-3443. https://doi.org/10.1002/mp.15568.

[26] Seymour, E.L., Downes, S.J., Fogarty, G.B., Izard, M.A., Metcalfe, P. (2011) In vivo real-time dosimetric verification in high dose rate prostate brachytherapy. *Med Phys.* 38(8):4785-94. https://doi.org/10.1118/1.3615161

[27] Johansen, J.G., Rylander, S., Buus, S., Bentzen, L., Hokland, S.B., Søndergaard, C.S., With, A.K.M., Kertzscher, G., Tanderup, K. (2018) Time-resolved in vivo dosimetry for source tracking in brachytherapy. *Brachytherapy*. 17(1):122-132. https://doi.org/10.1016/j.brachy.2017.08.009

[28] Debnath, S.B.C., Ferre, M., Tonneau, D., Fauquet, C., Tallet, A., Goncalves, A., Darreon, J. (2021) High resolution small-scale inorganic scintillator detector: HDR brachytherapy application. *Med Phys.* 48(4):1485-1496. https://doi.org/10.1002/mp.14727

[29] Allahverdi, M., Sarkhosh, M., Aghili, M., Jaberi, R., Adelnia, A., Geraily, G. (2012) Evaluation of treatment planning system of brachytherapy according to dose to the rectum delivered. *Radiat. Prot. Dosimetry*. 150(3):312-5. https://doi.org/10.1093/rpd/ncr415

Declaration of interests

☒ The authors declare that they have no known competing financial interests or personal relationships that could have appeared to influence the work reported in this paper.

☐ The authors declare the following financial interests/personal relationships which may be considered as potential competing interests: